Journal of Experimental Nanoscience
Publication details, including instructions for authors and subscription information:
http://www.informaworld.com/smpp/title~content=t716100757

Accurate velocity measurements of AFM-cantilever vibrations by Doppler interferometry

José F. Portolés[a]; Peter J. Cumpson[b]; John Hedley[c]; Stephanie Allen[a]; Philip M. Williams[a]; Saul J. B. Tendler[a]
[a] Laboratory of Biophysics and Surface Analysis, University of Nottingham, Nottingham, NG72RD, UK [b] Division of Quality of Life, National Physical Laboratory, Teddington TW11 0JT, UK [c] School of Mechanical and Systems Engineering, University of Newcastle, Newcastle-upon-Tyne NE1 7RU, UK

Online publication date: 28 September 2010

To cite this Article Portolés, José F. , Cumpson, Peter J. , Hedley, John , Allen, Stephanie , Williams, Philip M. and Tendler, Saul J. B.(2006) 'Accurate velocity measurements of AFM-cantilever vibrations by Doppler interferometry', Journal of Experimental Nanoscience, 1: 1, 51 — 62
To link to this Article: DOI: 10.1080/17458080500411999
URL: http://dx.doi.org/10.1080/17458080500411999

Journal of Experimental Nanoscience,
Vol. 1, No. 1, March 2006, 51–62

Taylor & Francis
Taylor & Francis Group

Accurate velocity measurements of AFM-cantilever vibrations by Doppler interferometry

JOSÉ F. PORTOLÉS†, PETER J. CUMPSON*‡, JOHN HEDLEY§,
STEPHANIE ALLEN†, PHILIP M. WILLIAMS† and SAUL J.B. TENDLER†

†Laboratory of Biophysics and Surface Analysis, University of Nottingham, Nottingham, NG72RD, UK
‡Division of Quality of Life, National Physical Laboratory, Hampton Road, Teddington TW11 0JT, UK
§School of Mechanical and Systems Engineering, University of Newcastle, Newcastle-upon-Tyne NE1 7RU, UK

(*Received September 2005; in final form October 2005*)

Doppler velocimetry is widely used in the measurement of nanometre resonance vibrations of micro-electromechanical systems (MEMS). It has excellent sensitivity and precision, but typical engineering applications do not require traceability of these velocity measurements to the SI system. While Doppler velocimetry is, in principle, easy to make traceable to the velocity of light, in practice a frequency-to-voltage conversion in common commercial instruments breaks this traceability unless calibrated. Typically, though, calibration is performed at a much lower frequency than those typical of MEMS devices, without the guarantee that the calibration is applicable in this higher frequency regime.

We present a method of traceable measurement of velocity in terms of the velocity of light, valid for the range of frequency and nanometre amplitudes typical of MEMS devices driven to resonance vibration. This is achieved by analysis of sideband amplitudes in the interference spectrum before demodulation of the Doppler signal. These sideband amplitudes can conveniently be measured using a benchtop spectrum analyser, a piece of widely available electrical test equipment. We illustrate the method with measurements on individual AFM cantilevers. In combination with cantilever calibration methods based on MEMS devices this method enables traceable calibration of those cantilevers employed for the measurement of pico- and nanonewton forces between individual biomolecules.

Keywords: AFM; Calibration; MEMS; Doppler; Vibration; Traceability

1. Introduction

An important class of micro-electromechanical systems (MEMs) device is the resonant sensor that measures a physical quantity through changes in the device resonance. These changes are in terms of resonance frequency, phase, quality factor or amplitude. An example of the latter is non-contact mode atomic force microscopy (AFM) imaging,

*Corresponding author. Email: peter.cumpson@npl.co.uk

Journal of Experimental Nanoscience
ISSN 1745-8080 print/ISSN 1745-8099 online
http://www.tandf.co.uk/journals
DOI: 10.1080/17458080500411999

where the microfabricated AFM cantilever is the MEMS device in question, and its amplitude of the cantilever resonance can be related to the dissipation of energy [1].

One important aspect regarding accuracy in the measurement of a physical quantity is traceability. Traceability to a metric system implies that the measurements can be expressed in terms of the physical units as they are defined in the metric system. Traceability is usually achieved by calibration of the instruments. However, it is immediately achieved when the measurement method is a primary method. This means when the measurements provided can be directly expressed in terms of physical constants which have fixed values in the units of the metric system. Resonance frequency measurements can be easily performed traceably to the SI system. However, traceable measurements of resonance amplitude are much more difficult. In a typical AFM, an optical lever is used to measure cantilever deflection, and requires a number of calibration steps before those deflections can be related to displacement of the tip or angular deflection of the cantilever. Sensitivity is high, but traceability is absent unless careful calibrations are made.

One type of device in which measurement of vibration amplitude is critical is the electrical nanobalance [2], a device for AFM spring-constant calibration that we have described previously. The calibration of the electrical nanobalance involves the measurement of a vibration amplitude typically in the range 10–15 nanometres, with an accuracy of around 1%. This is a challenge for conventional light interferometry. Doppler interferometry [3], however, allows the measurement of velocity amplitude with this precision [4, 5]. Doppler interferometry was employed initially in flow measurements [6, 7] and it has found a growing number of applications in research and industry. Examples are measurements of blood perfusion [8] in biomedical research and vibration measurements in the automotive industry [9, 10]. There are many possible designs for Doppler interferometers, depending on its application. Doppler interferometers can be built in the laboratory using bulk optical elements [11] but commercial equipment is usually based on optical fibres. In principle, since Doppler interferometry allows the velocity to be related directly to the speed of light, we have a primary method for velocity measurement of MEMs devices.

Doppler vibrometry is the application of Doppler velocimetry to the measurement of vibration phenomena. Not surprisingly therefore, Doppler vibrometry has become a widely used technique in the dynamic characterization of MEMs devices [2, 12–15], such as gyros, oscillators and accelerometers. Doppler vibrometry, as application of Doppler velocimetry, is in principle a primary method for the measurement of vibration velocity amplitudes. In practice, though, Doppler vibrometers usually have an analogue demodulation stage, converting the Doppler signal into an analogue voltage, and this frequency-to-voltage conversion needs calibration. Usually this is done by adjusting at a variable resistor, while applying the interferometer to the surface of a standard piezoelectric vibrator, almost always at 156 Hz. This is clearly well below the typical frequencies encountered in MEMs measurements, usually in the range of kHz.

In this paper we consider in detail the process of traceable measurement of velocity using Doppler vibrometry, for the range of frequency and amplitude typically encountered in MEMs devices. We show that with relatively simple measurements using a spectrum analyser, one can measure accurate and traceable velocities in the

millimetre-per-second range. For those quantities amenable to measurement using MEMs resonators this will allow a traceable measurement for the first time.

We begin by developing the theory for frequency modulation in the Doppler interferometer detector, showing how the signal is formed and the features in its frequency spectrum that can be related to the velocity of the MEMs structure. We then validate the method experimentally with measurements on a commercially available AFM cantilever, of a type that will be familiar to most practitioners of AFM.

An important practical consequence in the application of this method is that, in combination with cantilever calibration methods based on MEMS devices [2, 12, 13], this method enables traceable calibration of those cantilevers employed for the measurement of pico- and nanonewton forces between individual biomolecules [16, 17].

2. Theory

Figure 1 shows a schematic of the Doppler vibrometer used in our study. It is based on the Mach–Zehnder interferometer. The sample is placed on a vibrating stage where it is driven to vibration at its resonance frequency ω_{m}. The polarized light emitted by the laser source, a 632 nm He–Ne laser, is split into two different beams by a polarizing splitter BS1. One beam, the reference, is led by a prism through a Bragg cell that shifts its frequency by a constant offset $\omega_{\mathrm{Bragg}} = 40\,\mathrm{MHz}$. The second, the object beam, passes through the polarizing beam splitter BS2, then after being led into an optical fibre by an input coupler, it passes through a $\lambda/4$ plate and it is focused on the sample surface from which it is back-scattered. The reflected light follows the same way back to the splitter

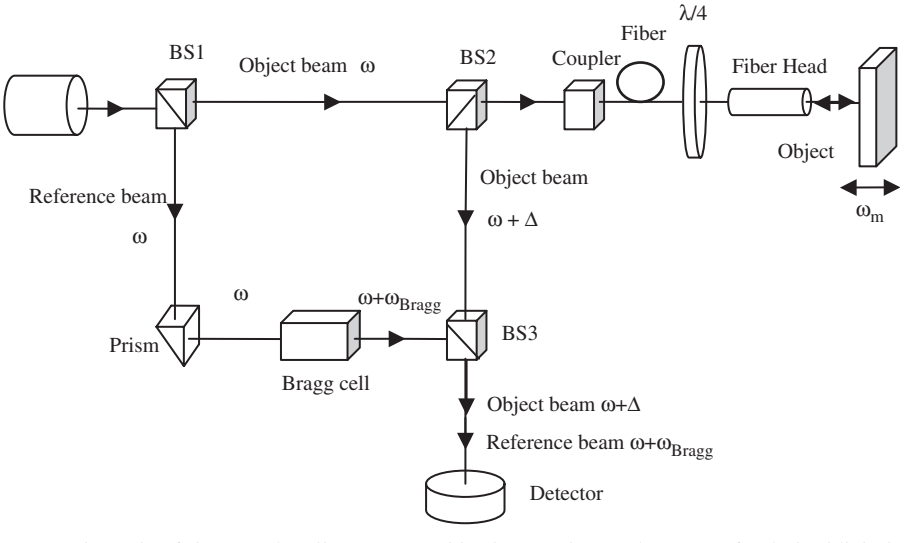

Figure 1. Schematic of the Doppler vibrometer used in the experiment. A source of polarized light is split into two beams. The Doppler signal containing information about the object vibration is recorded by the object beam as a modulation in frequency. The signal is extracted by demodulation from the interference of object and reference beam through demodulation.

BS2 where it is deflected to the polarizing splitter BS3. At the output from BS3 both beams have their electric fields summed. This results in an interference beam, the intensity of which is measured by a photodiode.

After reflection on the sample surface the object beam will be shifted in frequency by the Doppler effect due to the device vibration, producing a modulation in frequency (FM) on the reflected object beam [3]. The point of the device under the object beam vibrates with a time dependence given by

$$y = A\sin(\omega_m t) \tag{1}$$

The velocity of the point under study is then

$$\dot{y} = A\omega_m \cos(\omega_m t) \tag{2}$$

where $\dot{y}_{MAX} = A\omega_m$ is the velocity amplitude.

The associated Doppler frequency shift Δ or Doppler signal is given by [3, 8]:

$$\frac{\Delta}{\omega} = 2\frac{\dot{y}}{c} \tag{3}$$

where c is the velocity of light and ω the angular frequency of the laser.

From equation (2) it follows that the frequency shift has a harmonic time dependence:

$$\Delta = \Delta_0 \cos(\omega_m t) \tag{4}$$

with

$$\Delta_0 = 2\frac{\omega \dot{y}_{MAX}}{c}$$

The intensity of the interference beam is proportional to the square modulus of the resulting electric field [18], considering that the components of the electric field are in the same direction of polarization:

$$I(t) \propto |E(t)|^2 = |E_r(t) + E_t(t)|^2 = \left|E_r(t)\right|^2 + \left|E_t(t)\right|^2 + 2\mathrm{Re}\left\{E_r^*(t)E_t(t)\right\} \tag{5}$$

where E_r and E_t are the respective electric fields of the reference and object beams. The first two terms are independent terms each corresponding to one of the beams involved. The third one describes the interference between the two beams. Now the time dependences of these electric fields are

$$\begin{aligned} E_r(t) &= E_{r0} \exp i\left((\omega + \omega_{\mathrm{Bragg}})t\right) \\ E_r(t) &= E_{t0} \exp i\left(\omega t + \int_0^t \Delta(\tau)d\tau + \delta\right) \end{aligned} \tag{6}$$

where δ is a phase shift that arises due to the difference of optical paths between the two beams. Since optical paths are kept constant across the experiment, we can assume this phase shift to be constant and enclose it in the complex amplitude E_{t0}. The term $\int_0^t \Delta(\tau)d\tau$ accounts for the dependence of the phase on the frequency variations Δ(t) over time.

Given the harmonic time dependence of Δ (equation 4) and applying the theory of frequency modulation, $E_t(t)$ can be rewritten as [19]

$$E_t(t) = E_{t0} \exp i(\omega t) \sum_{n=-\infty}^{\infty} J_n(\beta) \exp(in\omega_m t) \tag{7}$$

where $J_n(\beta)$ is the nth-order Bessel function of the first kind [20], and $\beta \equiv \Delta_0/\omega_m$ is a parameter known as the modulation index.

Substituting equation (7) in equation (5) we obtain

$$\begin{aligned} \left|E(t)\right|^2 = \left|E_{r0}\right|^2 + \left|E_{t0}\right|^2 \left(\sum_{n,\,m=-\infty}^{\infty} J_n(\beta) J_m(\beta) \exp(i(n-m)\omega_m t) \right) \\ + 2\mathrm{Re}\left\{ E_{r0}^* E_{t0} \exp(-i\omega_{\mathrm{Bragg}} t) \sum_{n=-\infty}^{\infty} J_n(\beta) \exp(in\,\omega_m t) \right\}. \end{aligned} \tag{8}$$

Applying the Fourier transform in order to rewrite the expression in the frequency domain [21, 22] gives

$$\begin{aligned} F\left[\left|E_t(t)\right|^2\right](\omega) = \left|E_{r0}\right|^2 \delta(0) \\ + 2\pi \left|E_{t0}\right|^2 \sum_{n,\,m=-\infty}^{\infty} J_n(\beta)\, J_m(\beta) \delta(\omega - (n-m)\omega_m) \\ + 2\pi \left|E_{r0}\right| \left|E_{t0}\right| \sum_{n=-\infty}^{\infty} J_n(\beta) \exp\left(i \frac{\Phi\omega}{(\omega_{\mathrm{Bragg}} - n\omega_m)} \right) \\ \times \left[\delta(\omega + (\omega_{\mathrm{Bragg}} - n\omega_m)) + \delta(\omega - (\omega_{\mathrm{Bragg}} - n\omega_m)) \right]. \end{aligned} \tag{9}$$

The second term consists of a set of infinite sidebands found at frequency intervals of ω_m and centred around a central signal at $\omega = 0$. The amplitudes of the second-term sidebands are given by

$$A_k^{2ndterm} = 2\pi \left|E_{t0}\right|^2 \sum_{n=-\infty}^{+\infty} J_n(\beta)\, J_{n+k}(\beta) \tag{10}$$

Finally, the interference term is

$$2\pi \left|E_{r0}\right| \left|E_{t0}\right| \sum_{n=-\infty}^{\infty} J_n(\beta) \exp\left(i \frac{\Phi\omega}{(\omega_{\mathrm{Bragg}} - n\omega_m)} \right) \left[\delta(\omega + (\omega_{\mathrm{Bragg}} - n\omega_m)) + \delta(\omega - (\omega_{\mathrm{Bragg}} - n\omega_m)) \right]$$

where ϕ is the phase shift between reference and object beam. It consists of two sets of sidebands, one centred around $-\omega_{\text{Bragg}}$, the other around $+\omega_{\text{Bragg}}$. For $\omega_{\text{Bragg}} \gg \omega_m$ the first term can be ignored, since the magnitude of $J_n(\beta)$ decreases rapidly with n, and the interference term is approximated by

$$F[E_{\text{interf}}](\omega) = 2\pi \left|E_{r0}\right| \left|E_{t0}\right| \sum_{n=-\infty}^{\infty} J_n(\beta) \exp\left(i \frac{\Phi\omega}{(\omega_{\text{Bragg}} - n\omega_m)}\right) \times \delta(\omega - (\omega_{\text{Bragg}} - n\omega_m)) \tag{11}$$

Considering equation (11) and the property of Bessel functions [20]

$$J_{-k}(\beta) = (-1)^k J_k(\beta)$$

then the amplitudes of the interference sidebands, disregarding the phase $(-1)^k \exp[i\phi\omega/(\omega_{\text{bragg}} - n\omega_m)]$, are given by:

$$A_k^{\text{interf}} = 2\pi \left|E_{r0}\right| \left|E_{t0}\right| J_{|k|}(\beta) \quad (k = 0, \pm 1, \pm 2, \pm 3, \ldots) \tag{12}$$

Figure 2 shows a schematic of the amplitudes involved in the interference spectrum that we expect from equation (12).

Applying the recursive property of the Bessel functions [20]

$$\frac{2k}{\beta} J_k(\beta) = J_{k-1}(\beta) + J_{k+1}(\beta)$$

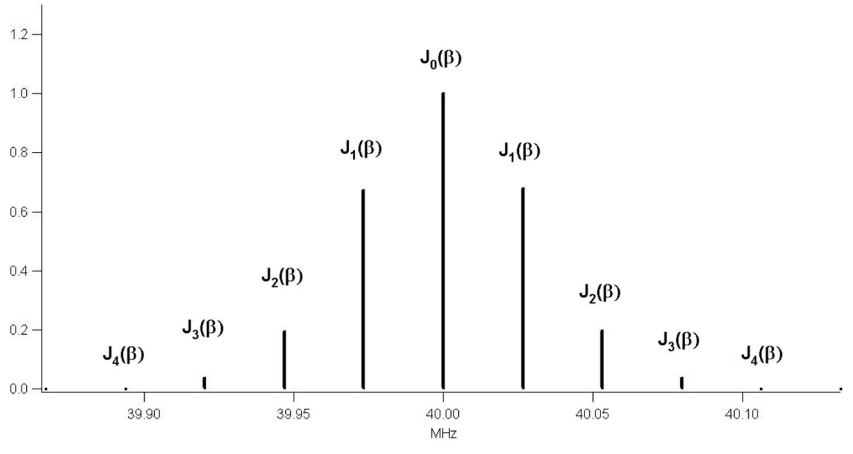

Figure 2. Sideband relative amplitudes in the interference spectrum. The relative amplitudes are proportional to values of the Bessel functions of the first kind of the modulation index involved in the Doppler signal.

to the case $k = 1$, we find the modulation index as a function of the first three Bessel functions:

$$\beta = 2\frac{J_1(\beta)}{J_0(\beta) + J_2(\beta)} \tag{13}$$

From equations (4), (12) and (13):

$$\dot{y}_{MAX} = \frac{1}{2}\frac{\beta\omega_m c}{\omega} = \frac{A_1^{\text{Interf}}}{A_0^{\text{Interf}} + A_2^{\text{Interf}}}\frac{\omega_m c}{\omega} \tag{14}$$

This expression gives the velocity amplitude of the MEMS device vibration in terms of the relative values of the first three sideband amplitudes. A special case is found for the first value of β at which $J_0(\beta) = J_1(\beta)$. This happens for approximately $\beta = 1.44$ [20].

3. Experimental measurements

A detailed description of this instrumentation has been published [2], so only the essential features will be summarized here. We used the Polytec OFV-3000 Laser Doppler vibrometer with an OFV-500 sensor head (Polytec GmbH, Waldbronn, Germany). In such Doppler vibrometers, the velocity and displacement measurement is carried out using a modified Mach–Zehnder interferometer. At this time the displacement output of the velocimeter was uncalibrated but expected to be linear, whereas the velocity signal had been calibrated by the manufacturer. The light source is a He–Ne laser that provides a linear polarized beam. A Bragg cell in the reference arm of the interferometer generates an additional frequency offset to determine the sign of the velocity. The resulting interference signal of the object beam and reference beam is converted into an electrical signal using a photo-detector and subsequently decoded in an electronic controller to provide analogue signals proportional to displacement and velocity. These signals were then analysed and displayed using a Hewlett–Packard 3562A Dynamic Signal Analyser (Agilent Technologies, Inc. Palo Alto, CA, USA).

In addition to the heterodyne-mixed velocity signal, this instrument model offers a direct output from the detection photodiode, labelled 'RF' on this instrument. A direct output from the photodiode might not be available in all the vibrometer models from Polytec. This is the signal whose frequency spectrum we analysed. Since the frequency offset introduced by the Bragg cell is 40 MHz, considerably larger than the bandwidth of the HP 3562A instrument, the signal was digitized using a National Instruments PCI 5112 card at 8-bit resolution and 100 MHz sampling (National Instruments, Austin, TX, USA), and transformed to the frequency domain using the built-in fast Fourier transform (FFT) [22] routine within the National Instruments Labview software (National Instruments, Austin, TX, USA).

In our measurements (figure 3) we used a microlever AFM-cantilever chip (Veeco Metrology, LLC, Santa Barbara, CA, USA). A white light interferometry micrograph can be appreciated in figure 4. This chip contains four triangular and one rectangular

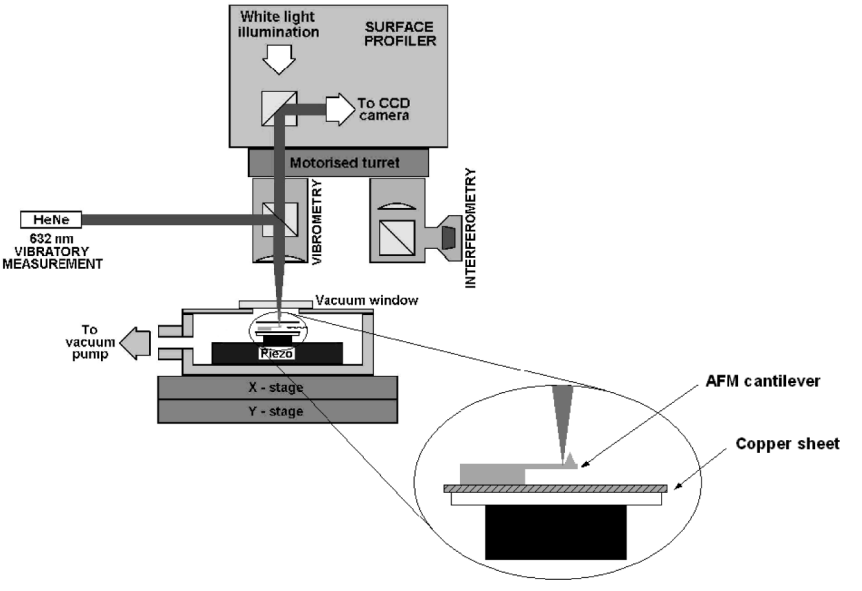

Figure 3. Experimental measurement of AFM cantilever resonance. The cantilever is placed in a vibrating stage. This is actuated by a piezo actuator. An harmonic ac voltage is applied to the piezo in order to bring the cantilever to resonance. The vibrating stage is placed inside a vacuum chamber in order to achieve high quality factors in the resonance curve. The optical setup enables simultaneous Doppler vibrometry and white light interferometry.

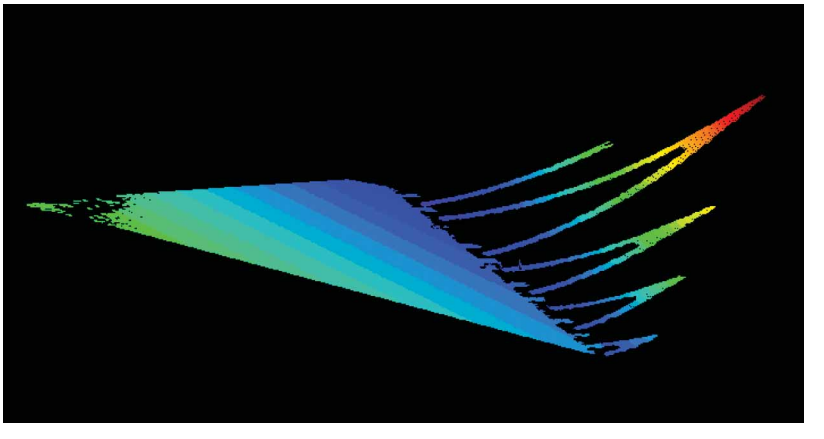

Figure 4. White-light interferometry topography map of the Microlever AFM cantilever chip, showing five cantilevers, including cantilever 'E', second from the bottom of this image. Note the upward curvature of the cantilevers, due to residual stress after manufacture. Cantilever E has a nominal length of 140 microns.

AFM cantilevers. We measured the vibration of the cantilever labelled 'E' by the manufacturer. This is the second longest triangular cantilever on the chip. The manufacturer provides a nominal value for the resonance frequency of 38 kHz with a minimum value of 26 kHz and a nominal value for the length of 140 micrometres.

We determined the resonance frequency of the cantilever to be 26.6 kHz. The measurements were performed driving the piezo-vibrator under the cantilever chip at this frequency.

We recorded a set of interference spectra raising the drive amplitude levels at uniform intervals of 50 mV. The data points in each peak were fitted to a Lorentzian function using the fitting algorithm built into the WaveMetrics Igor Pro 4.0.9 software package (Wavemetrics, Inc., Portland, OR, USA). The actual shape of the peaks is produced by the FFT algorithm [22] which applies a limited size window to the data sample previous to the conversion. This is translated in the frequency domain as a convolution of the sidebands with the Fourier transform of the applied window function, resulting typically in a sinc( ) function [21, 22]. The Lorentzian function was found to be a good approximation to the actual peak shape.

The heights of the three first peaks as measured on the fitted functions were used to obtain the modulation index and velocity amplitude for each drive voltage applying equations (13) and (14). From the obtained modulation indexes the corresponding values of the Bessel functions were calculated. From the theory the relative values obtained in this way should be in good agreement with the relative heights of the measured sidebands. In figure 5 the Bessel function values and the actual spectral data have been both normalized and superimposed for the drive voltage of 550 mV showing good agreement between the two sets of values. This is the maximum drive voltage achieved in the experiment, and the one that shows the most complex set of sidebands.

In the harmonic vibration, the velocity amplitude is proportional to the amplitude of the vibration, and this in turn is proportional to the amplitude of the harmonic drive signal applied to the piezo-actuator. Then, the velocity amplitudes are expected to show linear dependence with the drive voltages employed. The velocity amplitudes obtained with the sideband method are represented versus the corresponding drive voltages in figure 6 together with a linear fit. An estimation of the error committed in measuring the velocities with the sideband method arise from calculating the residuals of the measured velocities with respect to the linear fit. The root mean square of the residuals

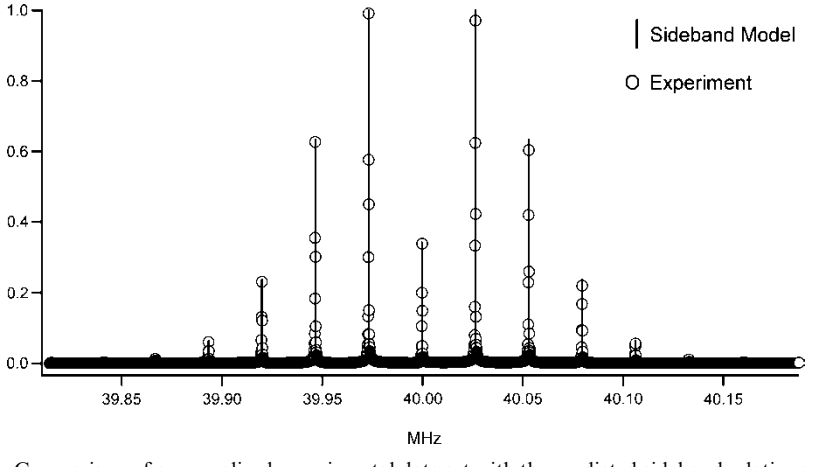

Figure 5. Comparison of a normalized experimental data set with the predicted sideband relative amplitudes (drive voltage = 550 mV).

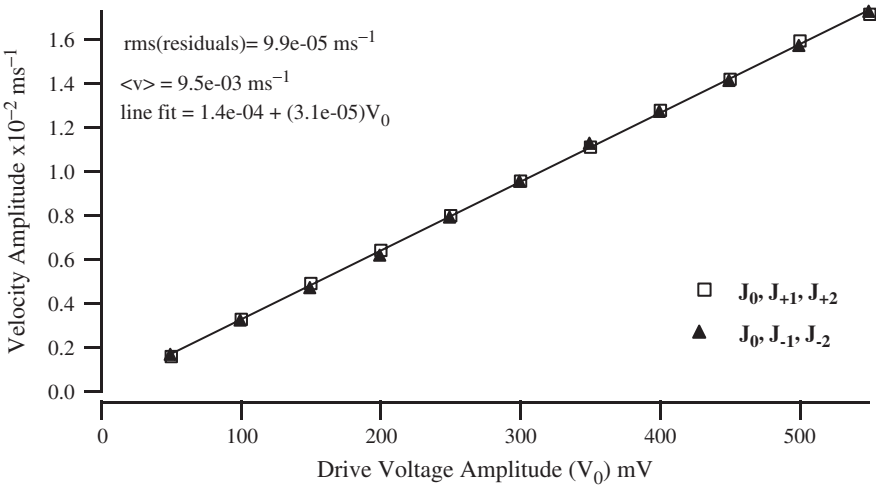

Figure 6. Velocity amplitude versus drive voltage. Squares represent velocities calculated from sidebands 0, +1, +2. The linear fit is calculated for the squares. Triangles represent the velocities from sidebands 0, –1, –2.

is found to be around 1% of the average of the measured velocities. The error estimation was performed for the velocities calculated from sidebands 0, +1, +2. The corresponding values for sidebands 0, –1, –2 are also displayed in figure 6. Since these velocity measurements are in terms of a fundamental constant with a fixed value within the SI system, this means that the measurement is traceable to the SI, and therefore that the accuracy of the measurement is equal to its precision.

4. Conclusions

We have described and tested a method to perform velocity measurements of MEMS device resonance vibrations, which is traceable to the SI. This method is based on heterodyne Doppler vibrometry and relies on direct measurements performed on the interference signal in the frequency domain using an spectrum analyser as an alternative to extraction of the Doppler signal by analogic demodulation. The analysis of the interference spectrum is based on the theory of frequency modulation. It predicts for the interference spectrum a set of sidebands located at regular frequency intervals equal to the frequency of the vibration, and relative amplitudes that are given by the whole set of Bessel functions of the first kind evaluated at the modulation index that characterizes the Doppler signal. The theory also provides the velocity amplitude of vibration directly in terms of the velocity of light through measurements of the relative amplitudes of sidebands that are present in the interference spectrum. A test was performed on a commercially available AFM cantilever. The cantilever driven at its resonance frequency for different drive voltage amplitudes show interference spectra that are in good agreement with the theoretic spectrum in all cases. From the observed spectra the corresponding velocity amplitudes of vibration were calculated. These results show a

consistent linear dependency with the drive voltage amplitudes employed and provide high accuracy in measurements of vibration velocity amplitude, traceable to the speed of light. We expect this approach to be important in characterizing AFM cantilevers as part of methods of spring-constant calibration for accurate pico- and nanonewton force measurements on single molecules.

Acknowledgements

José F. Portolés is grateful for a studentship funded by the National Physical Laboratory under its Strategic Research Programme, project 9SRPQ270. The authors are grateful to Tom Wiltshare and Mhairi Swann for valuable assistance during acquisition of the data.

References

[1] R. Garcia and R. Perez. Dynamic atomic force microscopy methods. Surf. Sci. Rep. **47,** 197 (2002).
[2] P. Cumpson and J. Hedley. Accurate force measurement in the atomic force microscope: a microfabricated array of reference springs for easy cantilever calibration. Nanotech. **14,** 918 (2003).
[3] L. E. Drain. *The Laser Doppler Technique* (Wiley, Chichester, 1980).
[4] M. Johansmann, G. Siegmund, and M. Pineda. Targeting the limits of laser Doppler vibrometry. http://www.polytec.com/int/_files/Idema_2005_Japan_Paper_Final.pdf.
[5] A. C. Lewin and G. Siegmund. Implications of system 'sensitivity' and 'resolution' on an ultrasonic-detecting laser Doppler vibrometer. SPIE Proceedings First International Conference on Vibration Measurements by Laser Techniques, **2358,** 292 (1994).
[6] H. Z. Cummins, N. Knable, and Y. Yeh. Observation of diffusion broadening of Rayleigh scattered light. Phys. Rev. Lett. **12,** 150 (1964).
[7] Y. Yeh and H. Z. Cummins. Localized fluid flow measurements with an He-Ne laser spectrometer. Appl. Phys. Lett. **4,** 176 (1964).
[8] J. D. Briers. Laser Doppler speckle and related techniques for blood perfusion mapping and imaging. Physiol. Meas. **22,** R35 (2001).
[9] W. Weber, M. Plieske, and G. Brauchle. Vibration measurements on a car transmission housing. SPIE Proceedings First International Conference on Vibration Measurements by Laser Techniques, **2358,** p. 359 (1994).
[10] B. Junge. Experiences with scanning laser vibrometry in automotive industries. SPIE Proceedings First International Conference on Vibration Measurements by Laser Techniques, **2358,** p. 377 (1994).
[11] O. J. Dussarrat, D. F. Clark, and T. J. Moir. The setting-up of an optical remote sensing system for target identification: a laboratory experiment. IEEE Trans. Educ. **42,** 3 (1999).
[12] P. Cumpson and J. Hedley. Accurate analytical measurements in the atomic force microscope: a microfabricated spring constant standard potentially traceable to the SI. Nanotech. **14,** 1279 (2003).
[13] P. J. Cumpson, P. A. Clifford, and J. Hedley. Quantitative analytical atomic force microscopy: a cantilever reference device for easy and accurate AFM spring-constant calibration. Meas. Sci. Technol. **15,** 1337 (2004).
[14] E. M. Lawrence, K. E. Speller, and D. Yu. Laser Doppler vibrometry for optical MEMS. Fifth International Conference on Vibration Measurements by Laser Techniques, Ancona, Italy (2002).
[15] J. F. Vigniola, X. Liu, S. F. Morse, B. H. Houston, J. A. Bucaro, M. H. Marcus, D. M. Photiadis, and L. Seharic. Characterization of silicon micro-oscillators by scanning laser vibrometry. Rev. Sci. Instrum. **73,** 3584 (2002).
[16] A. B. Patel, S. Allen, M. C. Davies, C. J. Roberts, S. J. B. Tendler, and P. M. Williams. Influence of architecture on the kinetic stability of molecular assemblies. J. Am. Chem. Soc. **126,** 1318 (2004).
[17] E. L. Florin. Sensing specific molecular interactions with the atomic force microscope. Biosensors & Bioelectronics **10,** 895 (1995).
[18] R. K. Wangsness. *Electromagnetic Fields*, 2nd ed. (Wiley, New York, 1986).
[19] B. A. Carlson. *Communication Systems*, Chapter 7, 3rd ed. (McGraw-Hill, New York, 1986).

[20] B. A. Carlson. *A Treatise on Theory of Bessel Functions*, 2nd ed. (Cambridge University Press, Cambridge, 1944).
[21] T. E. Jenkins. *Optical Sensing Techniques and Signal Processing* (Prentice-Hall, London, 1987).
[22] R. W. Ramirez. *The FFT: Fundamentals and Concepts* (Prentice Hall, Englewood Cliffs, New Jersey, 1985).